JOURNAL OF PROPULSION AND POWER
Vol. 26, No. 3, May–June 2010

Modeling, Simulation, and Controller Design for an Air-Breathing Combustion System

Kumar P. Bharani Chandra*
Coral Digital Technologies, Pvt., Ltd., Bangalore 560 043, India
Nitin K. Gupta†
IDeA Research and Development, Pvt., Ltd., Pune 411 013, India
N. Ananthkrishnan‡
Korea Advanced Institute of Science and Technology, Daejeon 305-701, Republic of Korea
and
I. S. Park§ and H. G. Yoon¶
Chungnam National University, Daejeon 305-764, Republic of Korea

DOI: 10.2514/1.42368

A novel, high-fidelity, low-order model is developed for an air-breathing combustion system designed for supersonic flight with a subsonic combustor. Detailed models for the individual components, intake, combustor, exhaust nozzle, and fuel supply system are interlinked by a low-order global model that captures the physics of the interaction between the intake and the subsonic combustor. Disturbances, both internal to the engine and external, due to atmospheric turbulence, are modeled. The terminal shock location in the intake duct is quantified in terms of the intake backpressure margin, called $P_{4\text{margin}}$. An innovative controller is designed that meets thrust demands with fuel flow rate and exhaust nozzle throat area as the two inputs, while maintaining a tight control on $P_{4\text{margin}}$ (intake shock location). Limits on fuel-air ratio, peak combustor temperature, fuel flow rate, and throat area actuator limits are imposed. The controlled combustion system is tested for an accelerated climb mission from a low altitude to a specified cruise Mach number and altitude. An outer guidance loop using dynamic inversion as a rapid prototyping tool is used for this test which, for a reference Mach command profile, provides the engine controller with the expected thrust demand at every instant. A closed-loop simulation is successfully demonstrated that takes the system through the acceleration phase to the desired cruise condition with a smooth switching between the acceleration and cruise segments.

I. Introduction

RAMJETS are the simplest form of air-breathing combustion systems in which the freestream air is compressed in the intake due to ram effect and allowed into a combustion chamber where fuel is introduced and combustion takes place. The hot gases, after combustion, are exhausted through a convergent–divergent nozzle, generating thrust. Ramjets have little or no moving parts; hence, they are simple, reliable, and provide reasonably efficient operation over a range of supersonic Mach numbers and altitudes. Ramjet-powered systems have been in operation for over a century and a detailed history of ramjet development, including a listing of ramjet systems developed, in progress, and planned, is provided by Fry [1].

The present paper describes a novel controller design for a ramjet-powered system that is required to be accelerated from 2.1 Mach at 1.4 km altitude to a 3.0 Mach, 14.5 km altitude cruise flight. Controller design is one of the key milestones in the development of an air-breathing combustion system [2,3], and some of the complexities involved in this effort are highlighted in the following paragraphs.

The primary purpose of the controller is to regulate the fuel flow to the combustion system so that the desired thrust is obtained at all flight conditions. This is done by regulating the signal to the fuel supply system (FSS), which then injects the desired quantum of fuel into the combustion chamber. At the same time the controller needs to ensure that no operating constraints are violated. The most crucial constraint is to ensure that the terminal shock remains inside the intake under all operating conditions, called supercritical operation. Under subcritical conditions, the terminal shock either comes out of the intake and sits on the nose cone, called unstart, or sets up a self-sustained oscillation, called buzz [4]. The other extreme is when the terminal shock is swallowed inside the combustion chamber, increasing the mean Mach number of the flow in the combustion chamber. This usually leads to a condition called flameout where the flame can no longer be maintained and gets extinguished. Both buzz and flameout need to be avoided, and the terminal shock location needs to be safely maintained inside the intake.

The terminal shock location can be difficult to quantify precisely from direct measurements as it may not necessarily be a single normal shock, but a supersonic tongue that extends deep into the intake [5]. Instead, the backpressure at the exit of the intake segment, which is far more amenable to accurate measurement, is used as it correlates well with the terminal shock location. In fact, too high a backpressure leads to the terminal shock being pushed out of the intake, whereas too low a backpressure can result in the terminal shock being sucked into the combustion chamber. Hence, the shock location constraint can be effectively handled by keeping a control on the intake backpressure. Typically, the forward-most position of the terminal shock, called the critical condition, and the rearmost position of the shock in the intake are noted in terms of the corresponding backpressure, and a safety margin of 10% in either

Presented as Paper 708 at the 47th AIAA Aerospace Sciences Meeting, Orlando, FL, 5–8 January 2009; received 2 December 2008; revision received 15 January 2010; accepted for publication 19 January 2010.

*Control Systems Engineer; bharanichandra@gmail.com.
†Chief Executive Officer; nitin@idearesearch.in.
‡Research Professor, Division of Aerospace Engineering; e-mail: drakn19@kaist.ac.kr.
§Senior Researcher, International Technology Cooperation Center; chardre@empal.com.
¶Project Manager, International Technology Cooperation Center; itcc_02@cnu.ac.kr.

direction is imposed. The quantum of the safety margin can be reviewed after extensive simulations and tests on actual hardware [6,7].

Another important parameter that needs to be constrained is the fuel-air ratio F/A. Too high values of F/A can cause high temperatures and pressures in the combustion chamber, leading to possible damage and failure. In any case, if F/A exceeds the stoichiometric value then the excess unburnt fuel is lost through the exhaust nozzle, making the operation inefficient. On the other hand, very low values will make it difficult to sustain the flame in the combustion chamber, leading to lean blowout (LBO) [8]. Estimate of F/A is possible as the fuel flow rate can be metered in the FSS, and the air flow entering the intake duct can be estimated from measurements by the air data system (ADS). The F/A itself needs to be different under acceleration and cruise conditions. During accelerated climb, the thrust should be enough to overcome drag and the weight component and still give the desired Mach number profile. This typically requires larger F/A. In fact, this is the phase where there is maximum risk of the intake going subcritical if there is a mismatch between the combustor pressure and the intake mass flow demand. At cruise, the thrust needs only be just enough to compensate for the drag, and F/A values are comparatively lower.

For ramjets that fly over a range of altitudes, the mass flow rate can change drastically from high values at low altitudes to low values at higher altitudes. A variable nozzle throat area is required to cater to this variation in mass flow rate, with the throat opened at lower altitudes but progressively closed as the system gains altitude. This functionality must also be provided by the controller. The nozzle throat area, assuming flow to be choked at the nozzle throat, directly controls the mass of combusted gas exiting from the nozzle. For a given intake mass flow, by varying the nozzle throat area and hence the nozzle exhaust gas flow, it is possible to manipulate the pressure in the combustion chamber, thus controlling the terminal shock location in the intake. Also, any change in the intake terminal shock location affects the total pressure recovery, which changes the total pressure at the combustor exit, and that affects the choking mass flow. The nozzle throat area variation, of course, has a small but significant effect on the thrust as well. Thus, a variable exhaust nozzle throat area can be a useful secondary control parameter, though the combined use of fuel flow and nozzle throat area is complicated by their mutual effects on thrust and intake backpressure.

The variable mass flow rate also implies that the fuel flow rate must change with altitude so as to keep F/A within desirable limits. This requires larger fuel flow rates at lower altitudes with decreasing fuel flow rates as altitude increases. Using a single fuel injection nozzle, it is difficult to achieve the entire range of fuel flow rates. Hence, two sets of fuel injectors, primary and secondary, are used, with both being kept open at lower altitudes to provide the larger fuel flow, but with only the primary kept on beyond a certain altitude. The controller must also perform this switching function properly.

When the system operates over a wide range of altitudes and Mach numbers, the system parameters also show large variations. Thus, a single set of controller gains will be inadequate to provide the desired performance. The traditional approach to this problem is to design several controllers for different operating points and then schedule the gains with a flight parameter, typically dynamic pressure or angle of attack. Each local controller can be designed using any method, such as proportional integral derivative (PID), linear quadratic gaussian/ loop transfer recovery (LQG/LTR), or H_∞. Because PID is a standard, well-understood method and widely used in the industry, it is the technique preferred for the work described in this paper [9,10].

PID controllers are model-based control design methods, that is, they need a good model of the combustion system dynamics to be available before control design. Computational fluid dynamics-based models can give an accurate description of the combustion system physics, but yield very high-order models that cannot be accommodated in controller design. On the other hand, low-order empirical models are easy to use for controller design, but do not capture the complex physical interactions in the combustion system. A novel, high-fidelity, low-order model for the air-breathing combustion system has been developed [11], wherein the detailed physics of each component of the combustion system is captured accurately, yet the overall combustion system dynamics is described by a low-order dynamical system. This model will be briefly described in the next section of this paper.

Any model, no matter what its fidelity, will have errors due to unmodeled dynamics and parameter uncertainties. In addition, combustion systems are noisy due to disturbances in the flow, shock-turbulence interaction in the intake [12], and combustion instabilities (acoustic phenomena due to interaction between the flow, the flame, and heat transfer in the combustion chamber) [13]. Shock-acoustic interactions in the intake could be due to bulk mode oscillations in the combustion chamber (included in the present model) and due to longitudinal, radial, or transverse acoustic modes (not considered presently) [14]. These phenomena are modeled in the form of disturbance models that introduce low-frequency disturbance in the intake backpressure due to heat release fluctuations in the combustion chamber, and a high-frequency disturbance due to turbulent interactions along the entire length of the combustion system. Fluctuations in the intake backpressure can be correlated to oscillations in the terminal shock location as well as to other flow variables. These disturbance models are also described in the next section of this paper. The controller design needs to be robust to account for uncertainties and disturbances. In the PID design technique, robustness is usually guaranteed by setting adequate gain and phase margins, which are then tested under simulation conditions.

The FSS that injects the fuel into the combustion chamber and the actuator that adjusts the nozzle throat area are themselves dynamical systems that need to be modeled. The FSS model is described in the Appendix. The FSS is known to introduce a delay of about 1 s in the system dynamics, which is usually unacceptable. The controller design, therefore, also needs to include a control for the fuel metering valve in the FSS. The throat area actuator model is usually a second-order transfer function with specified damping and frequency with saturation limits. The controller needs to operate under limits of fuel flow rate obtainable from the FSS and physical constraints on the nozzle throat area variation.

The controller design depends strongly on the availability of sensors to measure the variables required for use as feedback. The measured signal should adequately capture the dynamic coupling between the intake and the combustion chamber. This requires measuring a suitable variable at a location between the terminal shock in the intake duct and the nozzle throat downstream of the combustion chamber. Measurements in the combustion chamber or downstream are difficult due to the hostile environment and the variety of physical processes ongoing simultaneously in the combustor. The ideal variable to measure for feedback is the intake backpressure, and it can be measured by locating a set of pressure sensors at different streamwise stations upstream of the fuel injection station. As seen earlier, the backpressure also correlates well with the intake shock location, a key constraint parameter, and is the parameter that links the combustion chamber operating condition with the intake operation. Also, the various disturbances to be modeled can be incorporated as perturbations in the intake backpressure in the disturbance model. Thus, the PID controller design, which follows an output feedback strategy, uses intake backpressure as the feedback parameter to regulate two inputs, the fuel flow rate and the nozzle throat area. Additionally, critical intake backpressure, fuel flow rate, and throat area values are available to the controller, and measurements from the ADS (Mach number, altitude, dynamic pressure, and angle of attack) are used to schedule the gains and other parameters as a function of flight condition and for certain switching tasks.

The performance of the air-breathing combustion system with the controller can be tested by simulating flight along some reference trajectories. In particular, two flight segments need to be tested in the present instance, an acceleration segment from 2.1 Mach, 1.4 km to 3.0 Mach, 14.5 km, and a cruise segment at 3.0 Mach, 14.5 km. Following this, a typical combined acceleration-cum-cruise profile needs to be tested. To accommodate this, the controller should have an outer guidance loop with Mach command, where Mach number

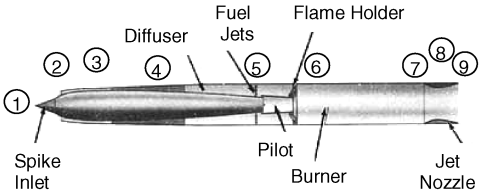

Fig. 1 Schematic of the air-breathing combustion system with station numbers marked.

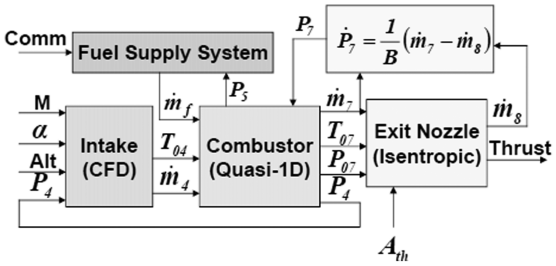

Fig. 2 Interface between different components of the global model.

measurements are assumed to be available from the ADS. However, in digital simulations, Mach number must be obtained by solving a differential equation involving the thrust and drag. In the present work, a dynamic inversion (DI) control law is used as a rapid prototyping tool to verify that the closed-loop combustion system does in fact meet the desired Mach profile during climb and cruise.

Besides optimizing the reference flight trajectory, which is outside the scope of the present work, several performance-improvement measures can be adopted for the combustion system by itself. For instance, in cruise, the fuel consumption can be cut down by choosing an appropriate combination of throat area and fuel flow rate that gives the same thrust. This automatically betters endurance/range for the given cruise Mach number and altitude. Again, efficiencies can be improved by stationing the terminal shock as far upstream as possible in the intake duct. This improves intake pressure recovery giving higher total pressures in the combustion chamber, and hence lower losses. At the same time, optimal performance must be weighed against the requirement of safety, especially in the presence of internal disturbances, atmospheric turbulence, and under off-design conditions. Attempting to hold the intake shock too close to the inlet of the duct under acceleration conditions may inadvertently cause the shock to become subcritical due to a surge of pressure in the combustion chamber. Too large a fuel injection rate during acceleration in climb (coupled with a decreasing intake mass flow rate) may result in F/A going over the limit and cause overtemperatures in the combustion chamber. The controller design should therefore provide for optimization or performance improvement, where possible, without violating any constraint or compromising safety.

The following sections will describe the combustion system model, the controller design philosophy and procedure, and give illustrative results of simulations to evaluate the closed-loop system performance. Following this, a complete simulation from beginning of acceleration phase to establishing the trim cruise flight will be demonstrated.

II. Modeling and Open-Loop Simulation

The air-breathing combustion system has an axisymmetric configuration and consists mainly of three components, an intake with a conical centerbody, a burner with liquid fuel injection and a flame-holder arrangement, and an exhaust nozzle, as shown in the schematic diagram in Fig. 1.** Stations 1–4 form the intake; station 2 is the cowl lip, and station 3 is the notional location of the terminal shock. Stations 4–7 represent the combustor; station 5 is the fuel injection point, and station 6 is the dump behind which the pilot flame is maintained. The exhaust nozzle extends from stations 7 to 9 with station 8 being the throat.

A novel low-dimensional dynamic model for the air-breathing combustion system has been developed [11]. Under this approach, each component (intake, combustor, and nozzle) has been modeled using an appropriate technique that adequately captures the complex physics in each case. The intake model is obtained from computational fluid dynamics (CFD) by using a Reynolds-averaged Navier–Stokes (RANS) code. A quasi-1-D code is developed to model the fluid mechanics and the reaction mechanisms for the combustor model. The nozzle is modeled as a simple isentropic component. The outputs of these models are stored in individual blocks (described below) in the form of tabular lookups or functional representation. The various component model blocks are then linked to each other in such a way that the physics of the system is truthfully reproduced to provide a low-dimensional model of the complete combustion system dynamics.

The interface between the various component blocks is depicted in Fig. 2. The key to the dynamical model is the block that updates the combustion chamber pressure P_7 based on the mass accumulation in the combustion chamber, i.e., the difference between the fuel plus air mass entering the combustion chamber and the gas mass exiting at the choked nozzle throat. This relation follows the work by Greitzer [15] for compression systems

$$\dot{P}_7 = \frac{1}{B}(\dot{m}_7 - \dot{m}_8) \tag{1}$$

where the backpressure factor B is given by

$$B = \left(\int_6^7 \frac{1}{\gamma RT(x)}\,\mathrm{d}x\right) A_{\mathrm{com}} \tag{2}$$

where A_{com} is the cross-section area of the combustor (between stations 6 and 7), and $T(x)$ is the static temperature at location x. B is one of the outputs from the quasi-1-D combustor code. The updated value of P_7 along with existing values at station 4 (not P_4) is used to read up values of other variables at stations 7, 5, and the intake backpressure P_4. The read-up value of P_4 is used to look up values in the intake block, and gets new values of other variables at station 4. On the next combustor block look up, these new station 4 values, with the latest update in P_7, result in revised values of the variables at stations 7, 5, and P_4. This is physically meaningful as the combustor, being subsonic, signals travel both upstream and downstream.

The delay in updating the system properties at various stations due to signal propagation, upstream and downstream, is modeled by a first-order dynamical system for each delay

$$\dot{x} = \frac{1}{\tau}(x_{ss} - x) \tag{3}$$

where x is the physical parameter, x_{ss} is its steady-state value read from a tabular look up or computed from a functional representation, and τ is the time constant. Each value of τ is computed by considering the appropriate signal speed to correctly capture the dynamics of the system. Time constants for nonacoustic variables being convected downstream with the mean flow velocity are computed as follows:

$$\tau_{i-j} = \int_i^j \frac{1}{u(x)}\,\mathrm{d}x \tag{4}$$

where i, j are station numbers, and $u(x)$ is the flow velocity at axial location x. Time constants for the upstream (or downstream) propagation of static pressure are obtained by considering acoustic waves traveling against (or with) the mean flow as follows:

$$\tau_{i-j} = \int_i^j \frac{1}{a(x) \mp u(x)}\,\mathrm{d}x \tag{5}$$

where $a(x)$ is the speed of sound at location x, $u(x)$ is the flow velocity at the same location, and the minus (or plus) sign represents

**Data available online at http://history.nasa.gov/SP-4404/app-b7.htm [retrieved 14 Nov. 2008].

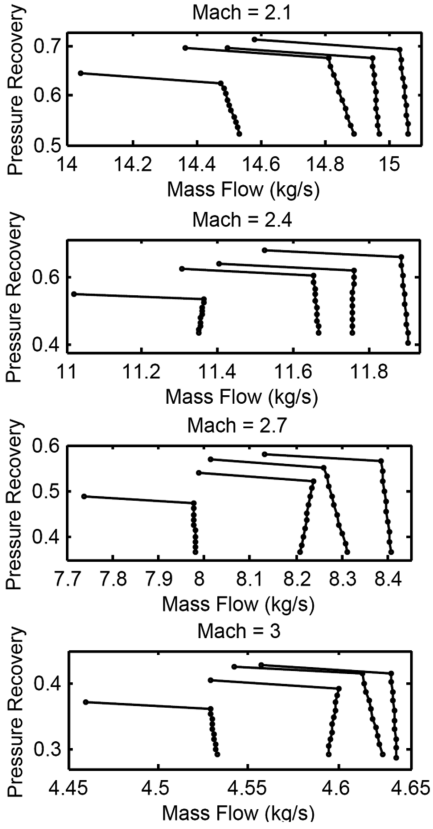

Fig. 3 Intake characteristics (AOA = 10, 5, 2, and 0 deg from left to right in each subfigure; circles correspond to different P_4 values).

the upstream (or downstream) propagating case, respectively. These time constants are also computed and tabulated in the combustor block.

A. Model Components

Intake: For each (Mach, altitude) combination, CFD simulations are conducted for different angles of attack (AOA = 0, 2, 5, 10 deg) and backpressure (P_4) values. The total pressure recovery (P_{04}/P_{01}), air mass flow rate, and backpressure (P_4) are recorded in tabular form after being suitably nondimensionalized. To speed up simulation runs, at the start of a series of simulations the intake tables are read and stored using Delaunay tessellations as a set of triangles such that no other data points are contained within the circle circumscribed by an individual triangle. During simulations, the triangulated data is searched to provide read-up values. The intake model in condensed graphical form is as shown in Fig. 3. The circles correspond to different P_4 values. The critical point (kink in each curve) is identified and a few subcritical operating points are also computed for each graph. For AOA = 0, the pressure recovery ranges from about 0.7 at 2.1 Mach–0.4 at 3.0 Mach, which is well within the expected range [16]. Also, for increasing AOA (for each Mach), the pressure recovery shows a fall, as expected, and a marginal decrease in the mass flow, consistent with the component of the stream-tube area entering the intake. The mass flow rates also show a variation of 3 times between the 2.1 Mach, 1.4 km case to the 3.0 Mach, 14.5 km case. For a given value of backpressure P_4 passed on from the combustor block, the intake block outputs the mass flow and total pressure at station 4, and $T_{04} = T_{01}$, which allows all other station 4 variables to be computed. In addition, the intake block also gives a measure of terminal shock location in terms of $P_{4\text{margin}}$, i.e., the difference between P_4 and its critical value, as shown schematically in Fig. 4. $P_{4\text{margin}}$ in percentage is defined as

$$P_{4\text{margin}} = \frac{P_{4\text{critical}} - P_4}{P_{4\text{critical}} - P_{4\text{lowest}}} \times 100 \tag{6}$$

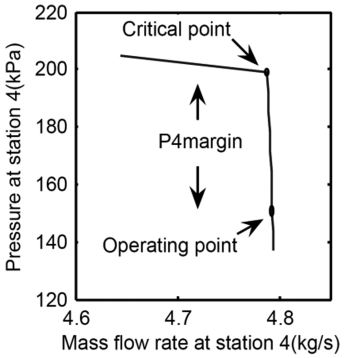

Fig. 4 Constraint on shock location, in terms of $P_{4\text{margin}}$.

where $P_{4\text{lowest}}$ is the P_4 at the lowest supercritical operating point in Fig. 4. $P_{4\text{critical}}$ represents the forwardmost limit of shock location in the intake duct, whereas $P_{4\text{lowest}}$ represents the rearmost limit of shock location in the duct. $P_{4\text{margin}}$ therefore directly correlates with shock location in the duct and can be used as the parameter to measure and control the shock location.

Combustor: The combustor model largely follows the work of O'Brian et al. [17] with some minor improvements. This involves solving a set of quasi-1-D equations for the gas dynamics in a variable-area combustor along with a detailed reaction mechanism for jet-A fuel consisting of 16 species and 23 reaction steps. Droplet injection, mixing, and evaporation are modeled for the fuel from both the primary (upstream injection) and secondary (downstream injection). A recirculation zone is assumed downstream of the dump at station 6 and heat and mass transfer across the shear layer forming its boundary is modeled. Frictional effects at the wall and at the recirculation zone boundary are accounted for, and heat loss through the walls is modeled by setting a wall temperature. The flame is assumed to be anchored at the base of the dump by way of a pilot injector and complete combustion is assumed in the recirculation zone, but unburnt fuel, if any, in the main flow is recorded at the combustor exit. The model is described in detail in [11]. The quasi-1-D combustor code outputs data into a table, as listed in Table 1. Several runs of the quasi-1-D code are carried out for various combustor inlet states and fuel injection conditions to generate the complete combustor table.

Exhaust Nozzle: The nozzle block uses isentropic flow relations to compute the choked mass flow through the throat

$$\dot{m}_8 = A_{\text{th}} \times \frac{P_{08}\sqrt{\gamma_8}}{\sqrt{RT_{08}}} \left(\frac{2}{\gamma_8 + 1}\right)^{\frac{\gamma_8+1}{2(\gamma_8-1)}} \tag{7}$$

where

$$P_{08} = r_n \times P_{07}, \qquad T_{08} = T_{07}, \qquad \gamma_8 = 1.2 \tag{8}$$

and $r_n = 0.98$. This block also calculates the thrust generated by the combustion system following the standard relations (e.g., see Farokhi [18]).

Fuel Supply System: The fuel supply system is separately described in the Appendix.

Throat Area Actuator: The actuator is modeled as a second-order system with a frequency of 9 Hz and a damping ratio of 0.6

Table 1 List of variables in combustor table

Station number	Variables
4	Mass flow rate, total temperature, static pressure
5	Fuel flow rate, total temperature, static pressure
7	Mass flow rate, total temperature, static pressure, total pressure, peak static temperature
Global	Time delay parameters, B parameter

$$TF_1 = \frac{3197.8}{s^2 + 67.9s + 3197.8} \tag{9}$$

Disturbances: Disturbances are modeled as pressure fluctuations and are introduced in the intake backpressure variable P_4, and from there they propagate to all the other system variables. They also result in oscillations of the terminal shock in the intake duct. One major source of disturbance in the combustion system is due to heat release fluctuations in the combustion chamber that drive the chamber acoustics [14]. Only the bulk acoustic mode is modeled here following the work in [19]. The combustion chamber of the air-breathing combustion system, with choked nozzle, behaves like a single bulk volume with a short neck. Helmholtz frequency ω_b associated with the bulk mode is given by

$$\omega_b = c\sqrt{\frac{A_n}{L_n V_b}} \tag{10}$$

where c is the speed of sound, A_n and L_n are the cross-sectional area and length of the neck, respectively, and V_b is the volume of the bulk. For the given combustion chamber, the Helmholtz frequency is estimated to be close to 30 Hz. This is modeled using a second-order transfer function with a frequency of 30 Hz and an estimated damping ratio of 0.1

$$TF_2 = \frac{35531}{s^2 + 37.7s + 35531} \tag{11}$$

The other major source of disturbance is due to turbulent fluctuations in the intake diffuser and the combustor, which is taken to be broadband noise and modeled as a low-pass filter with break frequency of 100 Hz. The transfer function for this appears as

$$TF_3 = \frac{394800}{s^2 + 754s + 394800} \tag{12}$$

Both disturbance models are excited by a Gaussian random function with zero mean and specified variance such that the perturbation due to turbulent fluctuations never exceeds 1% of P_4 at all frequencies and the perturbation due to the bulk mode never exceeds 5% at the resonant Helmholtz frequency of 30 Hz. These values are chosen based on the discussion in [14].

B. Constraints

The various constraints discussed earlier are also incorporated into the system model. Please note that the model does not actually impose the constraints on the system (that is the job of the controller), it merely records the constraint values.

Shock Location: Constraints on the shock location in the intake duct are specified in terms of the $P_{4\text{margin}}$ and are initially set at 10% (lower limit; forwardmost shock location) and 90% (upper limit; rearmost shock location). Violation of this constraint suggests the risk of either possible subcritical operation (lower limit) or flameout (upper limit). Later, depending on the system dynamic response as a function of flight condition, the controller may either impose tighter limits on the shock location or relax this constraint.

Fuel-Air Ratio: The upper limit on F/A is set at the stoichiometric ratio, which for jet-A comes to 0.0685. The lower limit to prevent LBO is set at 0.02 as recommended by [3]. In practice, neither F/A limit should normally be achieved as the corresponding $P_{4\text{margin}}$ constraint is likely to be attained earlier.

Maximum Combustor Temperature: The peak combustion temperature limit is set at 2200 K above which the combustor is likely to be damaged due to thermal effects [18]. The combustion temperature is related to F/A, and can be controlled by regulating F/A.

Fuel Flow Rate: The FSS limits the maximum and minimum amount of fuel per time that can be injected into the combustor. It also limits the maximum and minimum rate at which the fuel flow rate can be varied. This effect is captured in the detailed model of the FSS itself, so no additional constraints are required to be added.

Table 2 Trim values at 3.0 Mach, 14.5 km, 0 angle of attack

$m_{f\text{dot}}$	0.1982 kg/s	A_{th}	0.0335 m^2
P_4	173.3 kPa	$m_{4\text{dot}}$	4.7988 kg/s
P_{04}	187.0 kPa	T_{04}	607 K
P_7	162.7 kPa	$m_{7\text{dot}}$	4.997 kg/s
P_{07}	174.0 kPa	T_{07}	1909 K
$P_{4\text{margin}}$	25.7 kPa	Thrust	3196 N
F/A	0.0414	T_{peak}	1882 K

Throat Area Actuator: The mean value of the throat area is known to be 0.0335 m^2. A limit of $\pm 12\%$ variation in area about the mean value is modeled.

C. Open-Loop Simulations

Sample simulations are now carried out for the complete combustion system model, with disturbances included, to examine the response to each control input. The initial condition is a steady (trim) state at 3.0 m, 14.5 km altitude, with AOA = 0. Table 2 gives the trim values of the inputs and other important system variables. Results from two sets of simulations are shown in Fig. 5; in one case the throat area is held constant while the fuel flow rate is varied, in the other the fuel flow rate is held constant with throat area being varied.

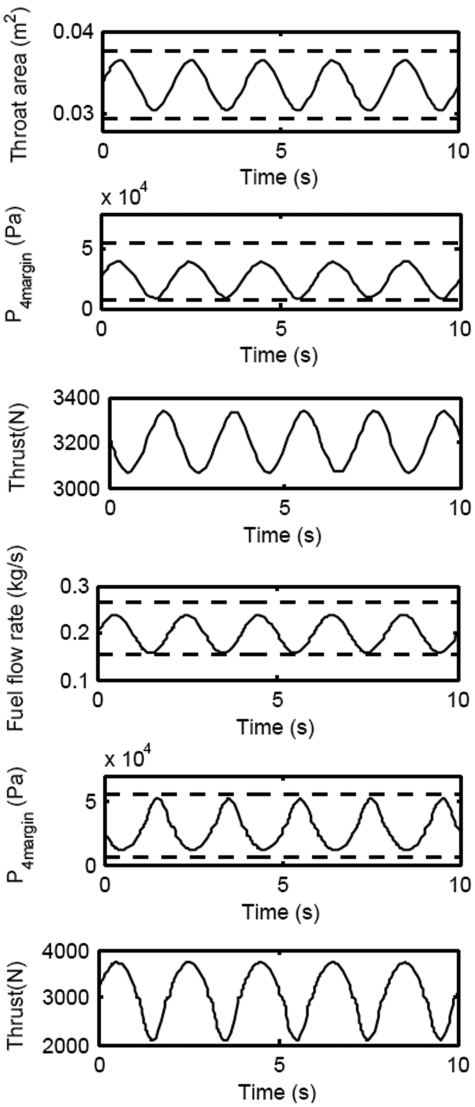

Fig. 5 Open-loop simulation with fuel flow rate (last three subfigures) and throat area (first three subfigures) as input (dashed lines indicate limits due to constraints).

The last three subfigures in Fig. 5 show the variation of $P_{4\text{margin}}$ and thrust with varying fuel flow rate input. The $P_{4\text{margin}}$ constraint boundaries are shown in the figure. The fuel flow rate is varied so that almost the entire range of $P_{4\text{margin}}$ is covered. Thrust modulation of about 1500 N is available over the range of allowable $P_{4\text{margin}}$ values. Likewise, the first three subfigures in Fig. 5 show the variation of thrust and $P_{4\text{margin}}$ with varying A_{th} input and fuel flow rate held constant. The limits on throat area here are the physical actuator limits. Varying throat area over nearly its complete range is seen to give significant modulation in $P_{4\text{margin}}$, but only a small range of thrust modulation of less than 300 N. An important lesson from this exercise is to appreciate that while fuel flow rate must be the primary control to attain the demanded thrust, throat area variation can be a useful secondary control to regulate the intake shock location or $P_{4\text{margin}}$.

In several hundreds of simulations carried out, neither the rich/lean limits on F/A, nor the peak combustor temperature limit was ever hit, suggesting that the $P_{4\text{margin}}$ (intake shock location) limits set the primary constraint for the system.

III. Controller Design

PID is a commonly used control design method that has found wide application and acceptance in industry [9]. When properly designed, the PID controller gives robust performance over a wide range of operating conditions. Both the design procedure and its operation are reasonably simple and straightforward, making it a popular choice. Typical PID control design is carried out for a linear, single-input–single-output, constant parameter system. The air-breathing combustion system model described here is, however, a multivariable, nonlinear system with parameters varying during flight. To apply the PID control design procedure to the air-breathing combustion system, one requires the following steps:

1. Choose a set of representative operating points over the flight envelop and derive linearized system models (one each with fuel flow rate and throat area actuator command as input) at each of these operating points. This is the system identification step.

2. Design PID controllers at each operating point for each control input. This involves tuning the three parameters for proportional, integral, and differential gains in each case to get the desired performance. This is the actual PID design step.

3. Put together the fuel flow rate and throat area controllers at each operating point so that any control demand is shared between the two of them using some logic. This is the control allocation step.

4. Schedule the gains as a function of one or more system parameters so that appropriate values of gains are obtained at all points of the flight envelop by interpolation between the representative operating points. This is the gain scheduling step.

A. Controller Design Philosophy

The proposed strategy for PID design of the air-breathing combustion system is shown in Fig. 6. Intake backpressure P_4 is the single measured variable. The critical value of P_4 is known (subject to computational uncertainties) from the intake CFD data, for various combinations of Mach number, altitude, and angle of attack. Thus, for every flight condition an estimate of $P_{4\text{margin}}$ is available. Given a $P_{4\text{margin}}$ command, the error between the commanded and estimated values of $P_{4\text{margin}}$ can be fed to the PID controller block, where (based on the control allocation logic) commands for the fuel flow rate and throat area will be produced. These will be given to the FSS (and its controller) and the throat area actuator, respectively, which will provide the inputs to the plant. This describes the inner stage 1.

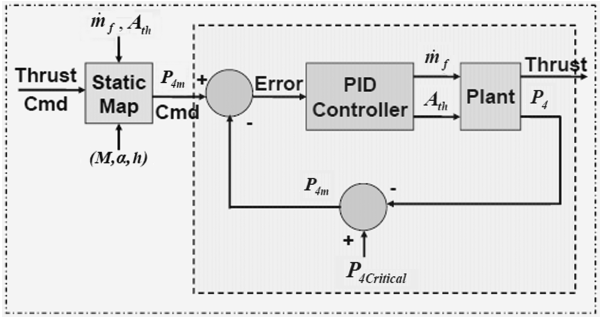

Fig. 6 Strategy for PID controller design.

Commanding $P_{4\text{margin}}$ has the advantage that the most critical constraint (intake shock location) is directly controlled, which also relates to the intake total pressure recovery. However, the system parameters of maximum relevance to performance are the thrust and a measure of efficiency, such as specific fuel consumption. The outer guidance loop (discussed later) will command a desired value of thrust. The key to the success of the present strategy is to map the commanded thrust to a $P_{4\text{margin}}$ command by a static map scheduled as a function of one or more flight parameters. This is done in the outer stage 2. In fact, the static map includes an explicit $P_{4\text{margin}}$ command limiter that ensures that the constraints on $P_{4\text{margin}}$ are never violated in the command.

A comment on the choice of control strategy. As there are two inputs available, an ideal control strategy could be to measure two outputs, each of which is fed back to regulate one each of the two inputs. In that case, intake backpressure measurement could be used to regulate throat area such that an optimal value of intake shock location is maintained, that is, $P_{4\text{margin}}$ control. This is also referred to as buzz margin control. To control thrust one could possibly estimate combustor total temperature. One way of doing this is to measure the static temperature at the nozzle throat, and knowing the throat Mach number to be sonic, calculate the throat total temperature, and knowing the combustor-to-throat area ratio, calculate the combustor exit total temperature. However, there are issues of sensing the nozzle temperature due to the location and the high temperature expected there of the order of 1800 K or higher. Therefore, questions of reliability, safety, and redundancy need to be addressed for this option. A more conventional option [2,3] is to use throat area feedback to control intake shock location (or backpressure) as before, but thrust commands are fed in the open-loop to regulate the fuel flow rate. This scheme suffers from obvious disadvantages of open-loop systems such as lack of robustness. Sudden changes in thrust command could cause surges in fuel flow rate that are not limited by $P_{4\text{margin}}$ limiters. Hence, there is a risk of subcritical operation if the throat area control for shock location does not respond quickly.

Instead, what is proposed in this work is a novel and innovative strategy where thrust can be controlled by using only a single measurement of intake backpressure. The key to this strategy is the thrust-to-P_4 mapping, which converts every thrust command to a $P_{4\text{margin}}$ command, which in the closed-loop regulates both fuel flow rate and throat area. The $P_{4\text{margin}}$ command limiter ensures that sudden changes in thrust command do not cause fuel flow rate surges. A huge advantage of this strategy is that it requires only one variable, static pressure of the cold air flow in the intake duct, to be measured.

B. Controller Design Procedure

In the following, the controller design procedure is carried out and tested by running two sets of simulations: one with a synthetic Mach command schedule for the acceleration segment, and the other with a $P_{4\text{margin}}$ command for the cruise segment.

1. *Selection of Operating Points*

The representative operating points for PID controller design are chosen based on the combustion system's expected flight profile and availability of aerodynamic data from prior analysis of intake and combustor, and are as listed in Table 3. The variation of throat area is to account for the varying mass flow rates at different flight conditions. Of the $\pm 12\%$ variation allowed in throat area, $\pm 6\%$ (approximately ± 0.02 m^2) is used for this purpose, while the rest is reserved for use in control to respond to the $P_{4\text{margin}}$ error signal. For the acceleration segment, throat area is fixed based on estimates of mass flow at different Mach numbers and altitudes. However, between Mach 2.7 and 3.0, throat area is not varied as F/A is being

Table 3 Operating points for proportional integral derivative controller design

Acceleration segment				Cruise segment			
Mach number	Angle of attack, deg	Throat area, m^2	$P_{4margin}$ command limiter, %	Mach number	Angle of attack, deg	Throat area, m^2	$P_{4margin}$ command limiter, %
2.1	0	0.0355	20	3.0	0	0.0315	6
2.4	0	0.0345	20	3.0	±2	0.0315	6
2.7	0	0.0335	10	3.0	±5	0.0315	6
3.0	0	0.0335	10	3.0	±10	0.0315	6

decreased, and also freestream temperature becomes a constant in the stratosphere. At cruise, throat area is decreased to the 6% limit of 0.0315 m^2.

For each operating point at which the linearized system for PID controller design is to be obtained, the trim value of thrust and corresponding values of $P_{4margin}$ and fuel flow rate need to be determined. This is done by selecting values of F/A. For the acceleration trims, F/A is picked as approximately 0.055 (as against a stoichiometric value of 0.0685) particularly to avoid violating the peak combustor temperature constraint. For the acceleration segment at Mach 3.0 and all points on the cruise segment, a lower F/A value of approximately 0.0414 is chosen. This is based on an estimate of thrust required at cruise to balance the drag at the expected trim condition. However, please note that this selection of F/A is only meant to pick a trim state for controller design. In operation, the control logic will allow larger or smaller values of F/A if demanded by the controller, subject to limits to avoid violating any constraint.

2. *System Identification*

Linearized models of the combustion system dynamics at each selected operating trim point are obtained in state space and transfer function form using the system identification tool box available with Matlab® [20,21]. The sequence of steps followed in this procedure is briefly listed below.

The combustion system model is first simulated in the open loop about each trim state by giving a judiciously selected synthetic input (to fuel flow rate or throat area, as the case may be) including a series of step functions and a combination of frequencies (sinusoidal and chirp signals) and constant offsets. This provides time series data of the input and output signals, which are imported from the Matlab® workspace into the SysId tool box after being suitably non-dimensionalized (e.g., fuel flow rate with intake mass flow rate, throat area with combustor cross-section area, and pressure margin with freestream static pressure). After suitable preprocessing one part of the data set, typically 50–60%, is selected as the working range for the estimation, while the other part is reserved for validation. Identification of linear models is done for orders from three to eight (number of states in the state space model). The linear models are then run using the validation input data to generate output that is matched with the validation output data. The fit percentage for various model orders is examined. Typically, too small an order will give a poor fit percentage, while too high an order will either show pole-zero cancellations and/or give an uncontrollable or unobservable system. For the present problem, fifth-order models gave the best fit (97.87%) and were found to be controllable and observable with no pole-zero cancellation.

The open-loop time response of the linear model is compared to that of the nonlinear plant to judge how well the linearized model actually captures the original nonlinear system dynamics about the trim point. The comparison is generally found to be good at the trim point with minor errors in peak over/undershoot and small mismatch in the steady-state values away from the trim, as expected. On checking the open-loop poles and zeros of the linear plant, the system is found to be stable but nonminimum phase (right half-plane zeros). The linear state space models are transformed into the frequency domain to obtain two transfer functions at each trim point, one each between fuel flow rate and throat area, respectively, and the $P_{4margin}$, for controller design. In case of throat area control, the system identification to generate linear models is carried out between physical (nondimensional) throat area input and (nondimensional) $P_{4margin}$ output. Then, the linear second-order actuator transfer function is appended to the identified linear plant, and PID controller design is carried out for the aggregated linear system between the actuator command input and $P_{4margin}$ output.

3. *Proportional Integral Derivative Control Design*

The PID design step involves choosing (tuning) the three gains in the transfer function below for each trim point

$$TF_4 = K_P + \frac{K_I}{s} + K_D s \tag{13}$$

where the subscripts P, I, and D stand for proportional, integral, and derivative, respectively. The tuning is done using standard methods, such as Zeigler–Nichols [22] or internal model control [23]. The gains are tuned to satisfy time-domain performance criteria, as follows: proportional control to adjust the rise time, integral control to eliminate the steady-state error, and derivative control to alter the overshoot. The time-domain performance of the PID controller is verified by giving various $P_{4margin}$ commands (small perturbation from trim, and large commands to upper and lower limiting values) and observing the response.

The fuel flow rate needs to respond to sharp changes in thrust command, and so the primary design criterion is the rise time. PID gains are tuned to ensure a rise time less than 0.05 s. Secondary design parameters are overshoot less than 10% of the magnitude of the step command and settling time less than 0.2 s. In case of throat area control, the primary design criterion is settling time of the order of 0.2 s, but with no overshoot. The overshoot could be an important factor when commanding trims near the lower $P_{4margin}$ limit. So tests for extreme values of $P_{4margin}$ (large deviation from trim) are carried out as the same set of gains designed for the trim $P_{4margin}$ are to be used across the entire range of $P_{4margin}$ values. The thrust response to throat area input does show an initial under/overshoot, whereas this behavior is not observed in the thrust response to fuel flow rate input. This is verified to be correct by analyzing the transfer function $G(s) - G(\infty)$ in each case, which shows one right half-plane zero in case of throat input, but none for the fuel flow rate input case [24].

Frequency domain criteria such as Bode plots for frequency response and gain and phase margins are then checked for acceptability. Gain margin of at least 6 dB and phase margin of at least 45 deg is maintained for all PID controller designs. Because the same time-domain criteria are maintained for all the trim conditions, the gain and phase margins differ from trim to trim, but all of them satisfy the minimum requirement above.

4. *Control Allocation*

For each operating point, two controllers have been designed about the chosen trim with fuel flow rate and throat area as input, respectively. Both controllers operate in parallel channels in the PID controller block in Fig. 6, and respond to the same $P_{4margin}$ command, and so a method to allocate the $P_{4margin}$ error signal between the fuel flow and throat area channels is necessary.

Fuel flow rate is the primary control effecter and has sufficient authority to cover the entire range of $P_{4margin}$ command values, whereas 50% of throat area control authority has been reserved for

trim variations, as discussed previously. Also, as seen earlier, the range of thrust variation obtained with throat area is limited. Notably, thrust shows a nonminimum phase (under/overshoot) response to throat area input. Hence, for good thrust tracking it would be desirable to filter out the low-frequency component of the error signal from the throat area channel and pass it only through the fuel flow rate channel. On the other hand, both throat area and fuel flow rate influence almost the entire range of $P_{4\text{margin}}$ values. After PID design, the closed-loop response of both inputs shows a settling time of similar order. However, fuel flow rate shows a very rapid response (small rise time) with overshoot, whereas throat area achieves tracking with no overshoot. Hence, throat area changes could possibly be beneficial in tracking higher frequency components in the $P_{4\text{margin}}$ error signal.

The control allocation scheme is therefore chosen as follows. The $P_{4\text{margin}}$ error signal is passed in full to the fuel flow rate channel, but a high-pass filter $H(s)$

$$H(s) = \frac{s^2 + 40s}{s^2 + 40s + 360} \tag{14}$$

with natural frequency about 3 Hz is introduced in the throat area channel. Another low-pass filter $L_1(s)$ with natural frequency about 6 Hz is introduced in the throat area channel to avoid undesirable response of throat area to high-frequency disturbance signals

$$L_1(s) = \frac{1420}{s^2 + 52.72s + 1420} \tag{15}$$

The PID controllers and the control allocation scheme are tested with a series of step $P_{4\text{margin}}$ commands, as shown in Fig. 7, which is seen to be well tracked with little under/overshoot and quick settling. Thrust tracking is also found to be good with very little delay. The control allocation scheme splits the $P_{4\text{margin}}$ error signal between the two channels, and both fuel flow rate and throat area show sufficiently rapid response when there are step changes in the $P_{4\text{margin}}$ command.

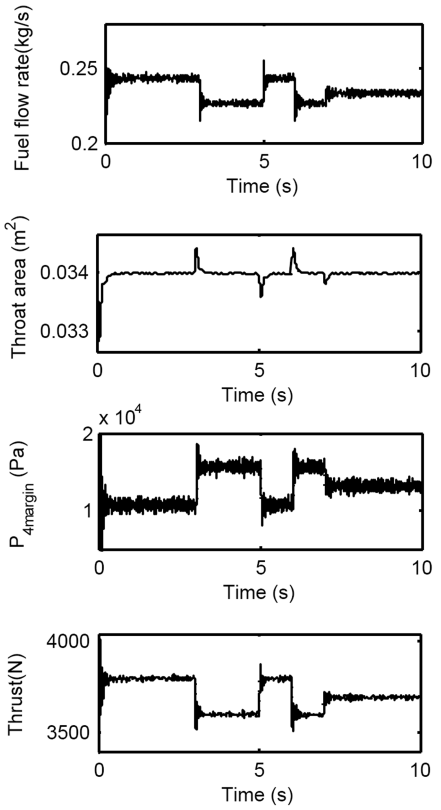

Fig. 7 Closed-loop simulation with fuel flow rate and throat area inputs mixed as per the control allocation scheme.

5. Gain Scheduling

During the acceleration segment all the PID gains, the trim setting of A_{th}, and the thrust-to-$P_{4\text{margin}}$ static map (to be discussed below) are scheduled as a function of freestream dynamic pressure

$$q_1 = 0.5\rho_1 V_1^2 = 0.5\gamma_1 p_1 M_1^2 \tag{16}$$

with $\gamma_1 = 1.4$. For cruise at 3.0 Mach, 14.5 km altitude, the gains are scheduled as a function of AOA. Both q_1 and AOA are expected to be available in flight from the ADS. All gains and scheduled parameters are obtained by linear interpolation between their values at the nearest operating points.

6. Thrust-to-$P_{4\text{margin}}$ Static Map

Thrust demands generated during flight need to be attained by the PID controller. Because the controller regulates $P_{4\text{margin}}$, a thrust command to $P_{4\text{margin}}$ command static map is used in stage 2 of Fig. 6 to achieve the desired thrust values. This is possible because for each operating point, there is a unique (single-valued) relationship between $P_{4\text{margin}}$ and thrust, with larger $P_{4\text{margin}}$ giving smaller thrust and vice versa. The procedure to obtain the static map for each operating point is by holding the throat area at its trim value, varying the fuel flow rate about its trim value, and noting down the pairs of values of $P_{4\text{margin}}$ and thrust. These are plotted in a graph and a suitable curve fit is done, which in all cases turns out to be a quadratic function. One such fit is obtained for each operating point, and these static maps are scheduled as a function of dynamic pressure q_1 during the acceleration segment and as a function of AOA during transition from acceleration to cruise.

The static map block also incorporates a $P_{4\text{margin}}$ command limiter. The command limiter plays a very important role by restricting the tendency for subcritical operation or lean blowout due to very large or very small thrust commands, respectively. In such cases the $P_{4\text{margin}}$ command limiter will provide as much or as little thrust as possible without sacrificing the safety of the system. Choice of $P_{4\text{margin}}$ command limiter values influences the performance of the system. A conservative choice of the command limiter settings will guarantee safe operation but will degrade the system efficiency because of higher total pressure loss obtained with larger $P_{4\text{margin}}$. On the other hand, choosing relatively tight values of $P_{4\text{margin}}$ will give higher efficiency, but there is a larger risk of subcritical operation, especially in the presence of disturbances (e.g., atmospheric turbulence) during the accelerated climb segment. Values for the $P_{4\text{margin}}$ command limiter are set as shown in Table 3 for different Mach numbers. $P_{4\text{margin}}$ command limiters are scheduled as a function of dynamic pressure during the acceleration segment and as a function of AOA during the switch from acceleration to cruise.

C. Closed-Loop Simulations

Simulations are now reported that test the closed-loop performance of the PID controllers designed, with the control allocation scheme, gain scheduling, and thrust-to-$P_{4\text{margin}}$ mapping, all incorporated.

1. Acceleration Segment

To test for the acceleration segment a synthetic Mach command is considered, as shown in Fig. 8. The corresponding values of thrust and fuel flow rate are found from open-loop simulations, as listed in Table 4. $P_{4\text{margin}}$ values are obtained from the static map in stage 2. Time histories are also reported in Fig. 8, which confirms that the static map generating the $P_{4\text{margin}}$ command and all aspects of the PID controller work satisfactorily during the acceleration segment. The few glitches during the ramp segments could be traced to the triangulated data lookup algorithm. The steep fall in fuel flow rate around $t = 10.5$ sec is due to injector switching; the same $P_{4\text{margin}}$ command is attainable with two different fuel flow rate values, and the controller automatically chooses the smaller value. The choice of lower F/A at Mach 3.0 makes sense because, as the freestream static

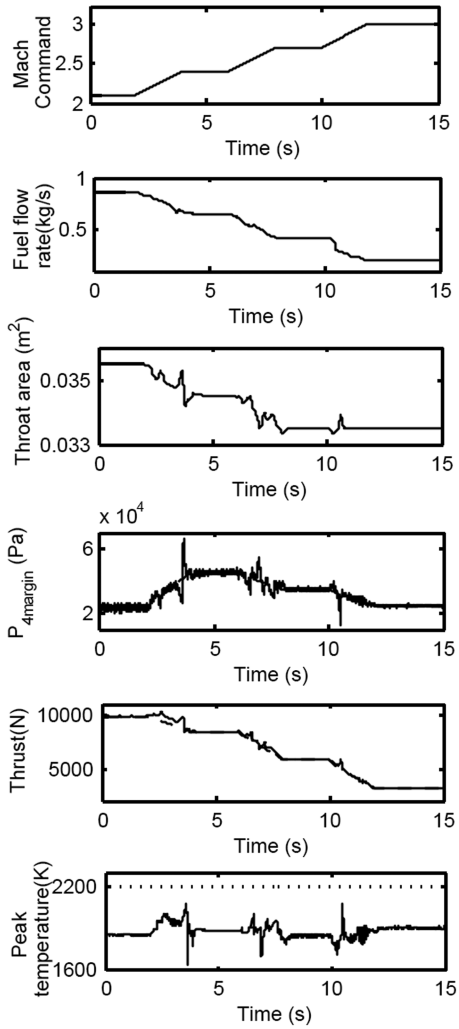

Fig. 8 Closed-loop simulation with synthetic Mach command for testing acceleration segment. In the thrust and P_4 margin plots dashed lines are commanded values, full lines are achieved values. The dotted line in peak temperature plot is the limiting value.

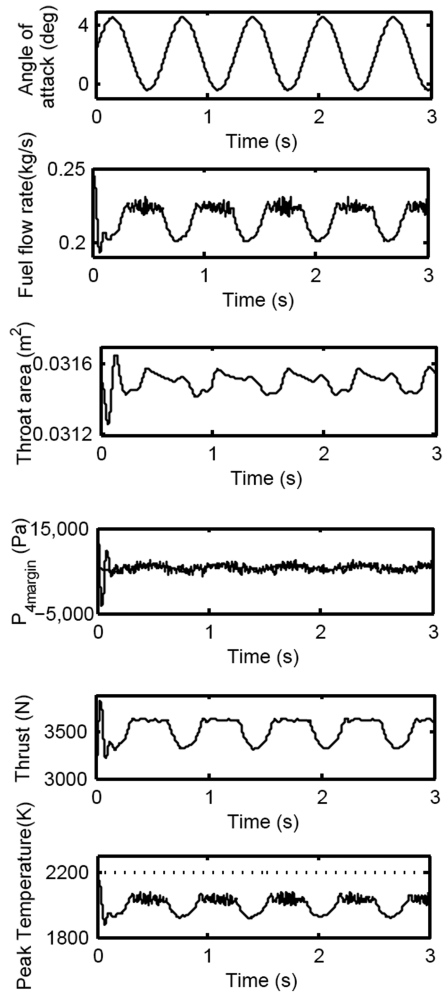

Fig. 9 Closed-loop simulation with $P_{4\text{margin}}$ command for testing cruise segment. In the P_4 margin plot dashed lines are commanded values, full lines are achieved values. The dotted line in the peak temperature plot is the limiting value.

temperature stops falling in the stratosphere, reducing the F/A is seen to keep T_{peak} under control.

2. Cruise Segment

To test the cruise segment, a synthetic AOA variation is considered with mean value of 2 deg and a sinusoidal variation of ± 2.5 deg over the mean at 1.6 Hz. For this simulation, $P_{4\text{margin}}$ command is directly given and is set at 10%, scheduled as a function of AOA. The gains and trim settings are also scheduled with AOA, and mean throat area is held at the reduced value of 0.0315 m^2. The AOA signal and simulation results are shown in Fig. 9. The $P_{4\text{margin}}$ command varies with time because the 10% value is different at different angles of attack. The PID controller is confirmed to perform well during cruise. The choice of 1.6 Hz frequency ensures that both fuel flow rate and A_{th} channels respond to $P_{4\text{margin}}$ error signals. The thrust response to the sinusoidal AOA variation shows a repeated plateau pattern because the thrust has nearly the same value over the AOA range of ± 2 deg.

IV. Mach Guidance Loop Design

While the PID controller appears to regulate all the combustion system parameters well, it needs to be confirmed that the controlled system meets the mission objective of accelerating to the correct cruise altitude and Mach number in the specified time of ~ 16 sec. For this purpose, an outer Mach guidance loop is designed using a DI control law as a rapid prototyping tool [25]. The error in Mach number is used by the DI law to compute the thrust desired to maintain the planned trajectory. The controller with the outer DI loop wrapped around it is shown in Fig. 10.

The estimated Mach number is obtained by integrating the thrust-drag balance equation

$$\dot{M}a = \frac{1}{m}(T - D - mg\sin\gamma) \tag{17}$$

Table 4 Values of variables corresponding to Mach schedule in Fig. 8

Mach number	Thrust, N	$P_{4\text{margin}}$, Pa, %	Fuel flow rate, kg/s	Fuel-Air ratio
2.1	9886	23433 [17.57]	0.8569	0.0570
2.4	8404	45537 [25.30]	0.6500	0.0552
2.7	5908	34824 [29.02]	0.4247	0.0516
3.0	3196	25690 [41.44]	0.1982	0.0414

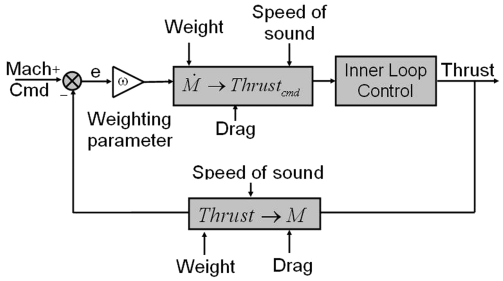

Fig. 10 Outer Mach guidance loop using a DI control law.

where a is the local speed of sound, m is the system mass estimated to be 124 kg, T and D are thrust and drag, and γ is the flight-path angle. Presently, $\gamma = 90$ deg, i.e., vertical climb, for acceleration segment, and $\gamma = 0$ for cruise, is assumed. Drag is calculated as

$$D = q_1 A C_D \tag{18}$$

where q_1 is the freestream dynamic pressure, A is the cross-sectional area using a diameter of 300 mm, and C_D is the drag coefficient, given by

$$C_D = C_{D_0} + C_{L_\alpha}\alpha^2 \tag{19}$$

with coefficients as given in Table 5. Using the available data, the cruise trim state at 3.0 Mach, 14.5 km altitude is estimated to be at an AOA of 2.063 deg, with thrust and drag value of 3615 N.

Then, based on the error between the commanded Mach number M_{cmd} and measured (estimated) Mach number, an $\dot{M}^{\text{desired}}$ value is computed as follows:

$$\dot{M}^{\text{desired}} = \omega_M (M_{\text{cmd}} - M) \tag{20}$$

where ω_M is a suitable weighting parameter that decides how fast/slow the outer loop response should be as against the inner loop response. Following standard practice [26,27], a typical value of ω_M for the present problem is ~ 2 rad/s. The desired $\dot{M}$ value is then used in the thrust-drag balance Eq. (17)

$$\dot{M}^{\text{desired}} a = \frac{1}{m}(T_{\text{cmd}} - D - mg\sin\gamma) \tag{21}$$

and inverted to get an equation for the commanded thrust T_{cmd}

$$T_{\text{cmd}} = \dot{M}^{\text{desired}} am + D + mg\sin\gamma \tag{22}$$

which is then fed to stage 2 of the PID controller.

A. Mach Command Profile and Switching Strategy

The desired Mach command profile is given by three piecewise linear segments (see Fig. 11). This one consists of a 5-s ramp from 2.1 to 2.8 Mach, followed by a 3-s ramp from 2.8 to 3.0 Mach, and a constant 3.0 Mach command thereafter. The break in the ramp at 2.8 Mach (approximately 11 km altitude) adjusts for the constant speed of sound in the stratosphere. It is expected that the system will achieve the desired cruise Mach number and altitude within 16 s.

Table 5 Aerodynamic data for drag calculation

Mach number	Altitude, km	C_{D_0}	$C_{L\alpha}$, deg
2.0	1.0	0.26	0.12
2.0	10.0	0.28	0.13
2.0	17.0	0.30	0.14
2.4	1.0	0.22	0.10
2.4	10.0	0.24	0.11
2.4	17.0	0.26	0.12
2.8	1.0	0.18	0.084
2.8	10.0	0.21	0.10
2.8	17.0	0.23	0.104
3.0	1.0	0.17	0.08
3.0	10.0	0.20	0.09
3.0	17.0	0.22	0.1

Next, a switching strategy between the acceleration and cruise flight segments is worked out. Because the ADS can provide a measure of altitude, it is ideal to start the switching strategy at a predetermined altitude. The height gained over 1 s of switching time can be estimated as

$$\frac{\mathrm{d}h}{\mathrm{d}\gamma} = \int_{90}^{0} \frac{V\sin\gamma}{\dot{\gamma}}\,\mathrm{d}\gamma \tag{23}$$

which works out to approximately 0.5 km of altitude during switching. On this basis, switching is initiated when the system reaches an altitude of 14 km, lasting 1 s. Denoting the altitude and time of initiation of switching as H^* and t^*, respectively, the parameters are scheduled during switching as listed in Table 6.

During switching, the PID gains and other scheduled parameters, such as thrust-to-$P_{4\text{margin}}$ command mapping, are computed as follows:

1) Interpolated cruise value: based on the AOA (between 0 and 2.063 deg), interpolation is done between the various Mach 3.0 cruise cases to get a value at cruise (call it C).

2) Interpolated acceleration value: based on the dynamic pressure, interpolation is done between the appropriate acceleration cases (usually Mach 2.7 and 3.0) to get a value at acceleration (call it A).

3) Final blended value: based on the bias throat area A_{th_b} setting, linear blending is done between the interpolated acceleration value and the interpolated cruise value to get a final blended value Y as follows:

$$Y(A_{\text{th}_b}) = 500 * [C * (0.0335 - A_{\text{th}_b}) - A * (0.0315 - A_{\text{th}_b})] \tag{24}$$

1. *Modeling Atmospheric Disturbance*

Atmospheric disturbance is a critical factor that may potentially lead to subcritical operation (or inlet unstart) [28]. Turbulent velocity fluctuations or gust is modeled using the Dryden Wind Turbulence Model, conforming to Mil Spec MIL-F-8785C [29]. Band-limited white noise is passed through an appropriate filter to produce the turbulent velocity spectrum. Transfer functions corresponding to positive vertical and lateral angular rate spectral components are considered. The turbulent velocity produced by this model is a function of altitude, velocity, and aircraft orientation specified in terms of a direction cosine matrix. Only the medium/high altitude case (over 2000 ft) is relevant for the present simulation. Assuming isotropic turbulence, the turbulence scale length is chosen to be 580 m for a wingspan (geometric characteristic length) of 1 m, and the turbulence intensity is set as severe. The rms turbulence amplitudes fall off with altitude, hence the effects of turbulent fluctuations are expected to be pronounced mainly at lower altitudes.

B. Design Case Simulation

The complete system with the given Mach command profile is now simulated for $t = 0$–12 s. The results are shown in Fig. 11. The commanded Mach profile is well tracked and the system perfectly attains the desired cruise trim state in a little over 10 s. The wind velocity due to atmospheric turbulence is seen to compare well with that in [27]. The most significant effect of the turbulent velocity fluctuations is seen in the low-altitude, low-Mach early acceleration phase where there are fairly severe shock ($P_{4\text{margin}}$) oscillations. Oscillations in F/A and thrust are also noticed over the same time period. This underscores the importance of including atmospheric turbulence in the overall model, and the conservative choice of $P_{4\text{margin}}$ limiter settings in Table 3 at lower Mach numbers. Even though atmospheric turbulence effects are not as severe at higher altitudes, fluctuations in $P_{4\text{margin}}$ and other variables persist because of the disturbances modeled in the combustion system.

The $P_{4\text{margin}}$ graph shows the demanded and actual values to be at the optimal minimum limit over nearly the entire flight time. Thus, an optimal $P_{4\text{margin}}$ or buzz margin control strategy is obtained during

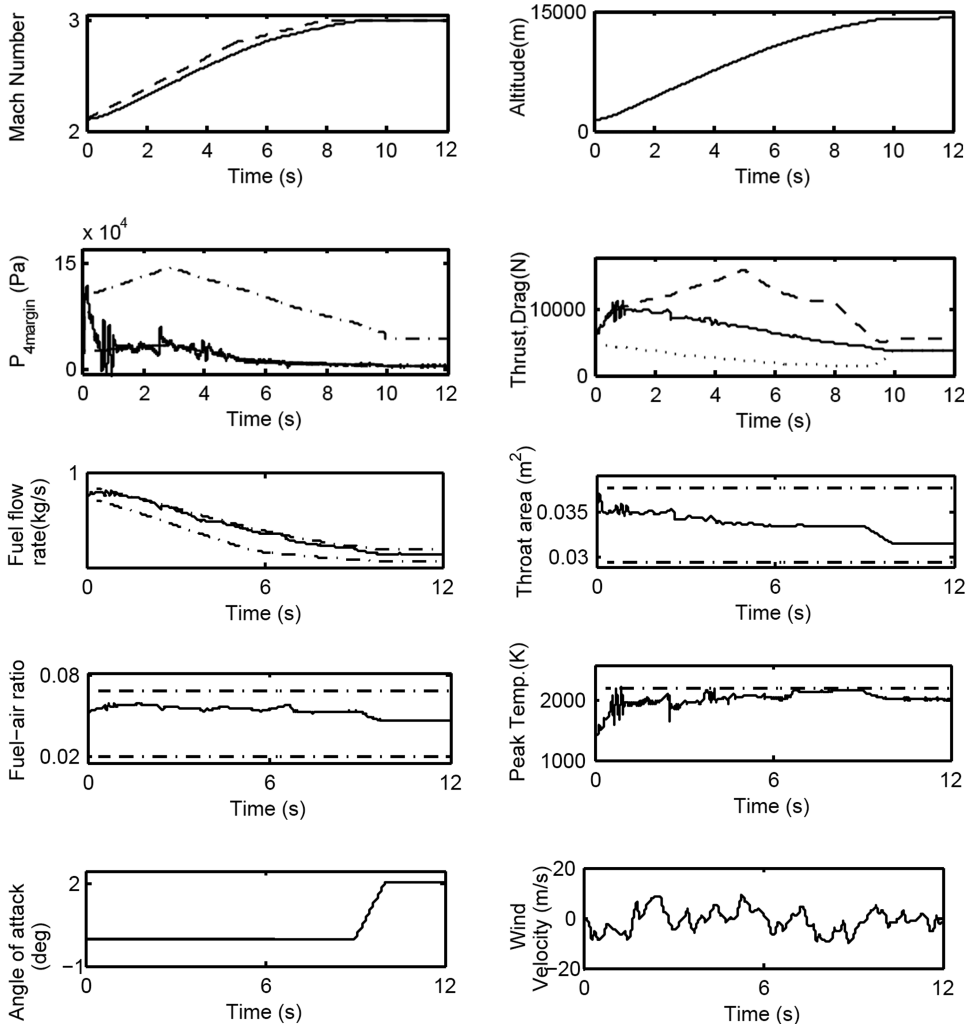

Fig. 11 Design case simulation with commanded Mach profile. The dashed lines are commanded values, dash-dot lines indicate limits due to constraints, and the dotted line in the thrust, drag plot is the drag.

the acceleration segment without explicitly stating it as a design objective. Consequently, the thrust available is the maximum value possible at each Mach number, and has been limited only by $P_{4\text{margin}}$ hitting the lower limit. The thrust-drag difference ensures that acceleration levels remains as high as possible, until the onset of switching where drag begins to rise with increasing AOA. Thus, the trajectory flown is expected to be very close to a minimum time-to-climb profile.

The F/A stays in the range of 0.05–0.06 over the entire acceleration segment, well below the stoichiometric limit. This is precisely the range of F/A values for the selected trim points for PID design. Thus, the system in fact operates close to the trim points for which the PID gains have been tuned. This is a positive aspect of the simulation. In fact, the fuel flow rate is, for the most part, very close to the upper limit, derived from the lower $P_{4\text{margin}}$ limit. This is responsible for maximizing thrust, as discussed above. The fuel flow rate falls steadily as the inlet mass flow rate decreases with altitude, with a sudden drop at the injector switching point of 0.36 kg/s. The lower-than-stoichiometric F/A also ensures that there is no unburnt fuel exiting from the nozzle, thus helping conserve fuel to extend the flight range in the cruise phase. The range of F/A values is also just correct as the peak combustor temperature stays in the 2000–2200 K range, just touching the 2200 K limit a few times. The lower LBO limit of $F/A = 0.02$ is never approached.

The mean throat area is gradually cut down from 0.0355 to 0.0335 m^2 during the acceleration phase to account for the decreasing mass flow rate with altitude. Additionally, there are fluctuations about the mean throat area in response to the $P_{4\text{margin}}$

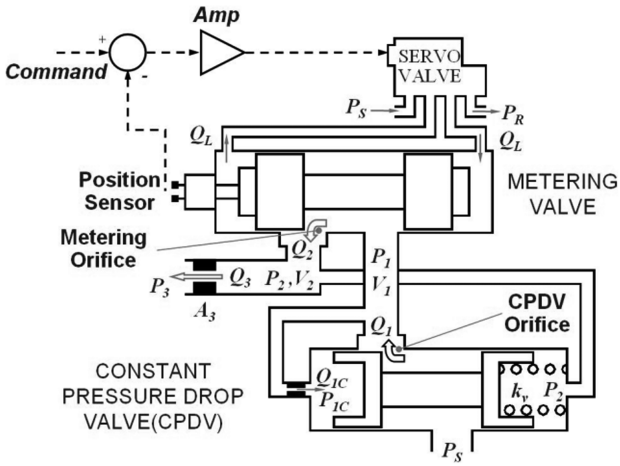

Fig. 12 Detailed schematic of the FSS.

Table 6 Parameter schedule during switching

Parameter	Start value ($H^* = 14$ km)	End value ($t^* + 1$ s)	Interpolation
Flight path angle γ	90 deg	0 deg	Linear
AOA	0 deg	2.063 deg	Linear
Bias throat area setting	0.0335 m^2	0.0315 m^2	Linear

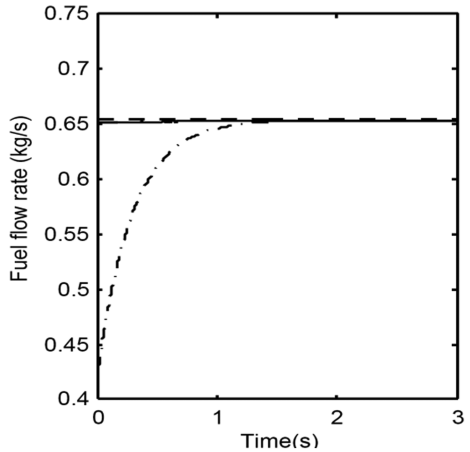

Fig. 13 FSS response to step input (dashed line), with (full line) and without (dash-dot line) controller.

error signal in the throat area channel, but the throat area actuator limits are not hit. The fuel flow rate too does not hit saturation limits due to the metering valve in the FSS, which is a good feature as the FSS controller (see Appendix) does not account for the nonlinearities due to saturation. It is desirable for the control actuators to avoid saturation as studies [30] have shown that actuator saturation causes the system to revert to open loop and there is a possibility of poor dynamic response or even instability in that case. The mean throat area is further cut down to 0.0315 m^2 during the switching period and the cruise phase, which allows the fuel flow rate to be reduced but still obtain the same $P_{4\text{margin}}$. This provides further saving in fuel consumption and also reduces the thrust marginally to eventually bring it down to the cruise value.

V. Conclusions

The main thrust of the present work has been to design a controller based on the traditional PID design technique for an air-breathing combustion system. With the intake backpressure margin $P_{4\text{margin}}$ as the output and with fuel flow rate and nozzle throat area as the input, two sets of PID controllers have been designed at various operating points. The operating points have been chosen based on the expected flight profile and available data points for (Mach, altitude) and AOA, and include an acceleration segment and a cruise segment. The two controllers have been blended using a control allocation scheme so as to respond to a single $P_{4\text{margin}}$ command. Thrust commands are taken in by converting them to an appropriate $P_{4\text{margin}}$ command using a static map. The choice of $P_{4\text{margin}}$ as the commanded variable allows tight control of the shock location in the intake duct, a critical constraint. The thrust-to-$P_{4\text{margin}}$ map function also includes a $P_{4\text{margin}}$ command limiter to prevent inadvertent constraint violations. The PID gains, trim settings, and the static map are scheduled as a function of dynamic pressure during acceleration and AOA for cruise. The use of a static map to convey the thrust command to an inner loop closed on $P_{4\text{margin}}$ is an innovative development that makes command tracking and stability to disturbances simultaneously possible with a single measurement of intake backpressure. The key to this entire effort has been the availability of a high-fidelity, low-order dynamical model of the air-breathing combustion system, reported in [11], including disturbances both internal and external to the engine and a fairly detailed FSS model.

An outer Mach guidance loop is designed using DI as a rapid prototyping tool to quickly verify that the controlled system does indeed meet the mission goals. Given a Mach command, the outer DI guidance loop commands a desired value of thrust that is passed on to the inner loop. The inner PID control loop has been separately tested for the acceleration and cruise segments; then with the outer loop closed, the entire closed-loop system has been tested for the desired Mach command profile with a smooth transition from the acceleration segment to the cruise segment. All the key parameters are seen to function correctly and the system is effectively accelerated from 2.1 Mach, 1.4 km altitude to cruise at 3.0 Mach, 14.5 km altitude without violating any constraint. The controller performance under off-design and disturbance conditions has also been evaluated to test for stability and robustness against disturbances and uncertainties; these results have not been reported here for lack of space.

Appendix: Fuel Supply System

The function of the fuel supply system (FSS) is to inject the desired amount of fuel into the combustor, and maintain the desired fuel flow rate under varying combustion chamber conditions. A schematic of the FSS is shown in Fig. 12.

I. Fuel Supply System Model

The various FSS subsystems to be modeled can be identified as:

1) The metering valve, which positions a servo valve based on the input command signal to control the area of the metering orifice thereby regulating the fuel flow rate.

2) The constant pressure drop valve (CPDV), which draws fuel from the air turbo pump (ATP) and maintains a near-constant pressure drop across the metering orifice by adjusting the position of a spring-loaded spool.

3) The ATP, which provides fuel to the CPDV.

4) The injector, which injects the desired amount of fuel into the combustion chamber. This consists of a primary and a secondary injector located at station 5 and a pilot injector at station 6 behind the dump for flame holding.

A. *Constant Pressure Drop Valve Model*

The purpose of the CPDV is to maintain the pressure difference across the metering orifice $\Delta P = P_1 - P_2$ at a near-constant value. This is done by manipulating the position of the spring-loaded spool, whose motion is modeled as

$$m_1\ddot{x}_{v1} + c\dot{x}_{v1} + k_s x_{v1} = A_{\text{CPDV}}(P_2 - P_{1c}) \tag{A1}$$

with the following constraint equations:

$$\begin{aligned} &Q_1 = C_D x_{v1} w_1 \sqrt{P_s - P_1} \qquad Q_2 = C_D x_{v2} w_2 \sqrt{P_1 - P_2} \\ &Q_3 = C_D A_3 \sqrt{P_2 - P_3} \qquad Q_{1c} = C_D A_{1c} \sqrt{P_1 - P_{1c}} \\ &Q_2 = Q_1 - Q_{1c} \qquad Q_2 = Q_3 - Q_{1c} \qquad Q_{1c} = \rho A_{\text{CPDV}} \dot{x}_{v1} \end{aligned} \tag{A2}$$

where the different variables are as labeled in Fig. 12. The damping coefficient is taken as $c = 32.3$ and the value of C_D, the discharge coefficient, is estimated to be 0.04.

B. *Air Turbo Pump Model*

The supply pressure from the ATP P_s is known to be a quadratic function of the flow rate Q_1 as follows:

$$P_s = 6.89655e6 * (-0.0004 * Q_1^2 + 0.0025 * Q_1 + 1.6813) \tag{A3}$$

C. *Metering Valve Model*

The metering valve controls the opening of the metering orifice x_{v2} by way of a Moog 30 series servo valve whose transfer function (flow rate to supplied current) is given by

$$\frac{Q(s)}{i(s)} = \frac{K_c \omega_n^2}{s^2 + 2\zeta\omega_n s + \omega_n^2} \tag{A4}$$

where $K_c = 2.4$, $\omega_n = 1507.96$, and $\zeta = 0.5$. The servo valve operates in a closed loop with negative feedback based on position sensed by the position sensor in Fig. 12. Position limits on the displacement of the metering and CPDV valves limit the fuel flow rates. These introduce nonlinearities in the system. The control strategy is aimed at never encountering these limits; hence a linear PID controller for the FSS should be adequate.

II. Fuel Supply System Controller and Simulation

The input to the FSS is a current signal. However, for purpose of comparison with the closed-loop system response, it is desirable to test the FSS open-loop performance for fuel flow rate input signals. To do this, first a static map is created between the FSS current input signal and the fuel flow rate. During simulations, for a fuel flow rate command this static map is inverted to find the corresponding current signal, which is then fed to the FSS to generate the actual fuel flow rate.

A standard PID controller with fuel flow rate feedback is designed. Based on the error between the commanded and measured values of fuel flow rate, proportional action is added to adjust the rise time and integral action is used to get zero steady-state error. The objectives are to have zero overshoot and a settling time roughly one tenth of the fuel flow rate and throat area PID controller settling times. That is roughly one tenth of 0.2 s.

The composite plot in Fig. 13 shows open-loop response to a step command in fuel flow rate, which indicates an unacceptably large time delay of about 1.5 s. In contrast, the closed-loop system with the PID controller shows a very good response with settling time of the order of 0.02 s and no overshoot.

References

[1] Fry, R. S., "A Century of Ramjet Propulsion Technology Evolution," *Journal of Propulsion and Power*, Vol. 20, No. 1, Jan.–Feb. 2004, pp. 27–58. doi:10.2514/1.9178

[2] Boksenbaum, A. S., and Novik, D., "Control Requirements and Control Parameters for a Ram Jet with Variable-Area Exhaust Nozzle," NACA RM E8H24, Nov. 1948.

[3] Harner, K. I., and Patrick, J. P., "Control Systems Requirements for Advanced Ramjet Engines," *AIAA/SAE 14th Joint Propulsion Conference*, AIAA, New York, July 1978.

[4] Trimpi, R. L., "A Theory for Stability and Buzz Pulsation Amplitude in Ram Jets and an Experimental Investigation Including Scale Effects," NACA Rept. 1265, Jan. 1956.

[5] Zha, G.-C., Smith, D., Schwabacher, M., Rasheed, K., Gelsey, A., Knight, D., and Haas, M., "High-Performance Supersonic Missile Inlet Design Using Automated Optimization," *Journal of Aircraft*, Vol. 34, No. 6, 1997, pp. 697–705. doi:10.2514/2.2241

[6] Ohshima, T., Kanbe, K., Kimura, H., Fujiwara, K., Suzuki, K., and Yanagi, R., "Control of the Intake Shock Position in the Test Rig for Ramjet Engine," *AIAA/ASME/SAE/ASEE 33rd Joint Propulsion Conference and Exhibit*, AIAA Paper 1997-2885, Reston, VA, July 1997.

[7] Kojima, T., "Experimental Study on Restart Control of A Supersonic Air-Breathing Engine," *Journal of Propulsion and Power*, Vol. 20, No. 2, March–April 2004, pp. 273–279. doi:10.2514/1.9253

[8] Prior, R. C., Fowler, D. K., and Mellor, A. M., "Engineering Design Models for Ramjet Efficiency and Lean Blowoff," *Journal of Propulsion and Power*, Vol. 11, No. 1, Jan.–Feb. 1995, pp. 117–123. doi:10.2514/3.23848

[9] Ang, K. H., Chong, G., and Li, Y., "PID Control System Analysis, Design, and Technology," *IEEE Transactions on Control Systems Technology*, Vol. 13, No. 4, July 2005, pp. 559–576. doi:10.1109/TCST.2005.847331

[10] Li, Y., Ang, K. H., and Chong, G., "PID Control System Analysis and Design," *IEEE Control Systems Magazine*, Vol. 26, No. 1, Feb. 2006, pp. 32–41. doi:10.1109/MCS.2006.1580152

[11] Gupta, N. K., Gupta, B. K., Ananthkrishnan, N., Shevare, G. R., Park, I. S., and Yoon, H. G., "Integrated Modeling and Simulation of an Air-breathing Combustion System Dynamics," *AIAA Modeling and Simulation Technologies Conference and Exhibit*, AIAA Paper 2007-6374, Reston, VA, Aug. 2007.

[12] Matsuo, K., and Kim, H. D., "Normal Shock Wave Oscillations in Supersonic Diffusers," *Shock Waves*, Vol. 3, No. 1, 1993, pp. 25–33. doi:10.1007/BF01414745

[13] Venkataraman, K. K., Preston, L. H., Simons, D. W., Lee, B. J., Lee, J. G., and Santavicca, D. A., "Mechanism of Combustion Instability in a Lean Premixed Dump Combustor," *Journal of Propulsion and Power*, Vol. 15, No. 6, Nov.–Dec. 1999, pp. 909–918. doi:10.2514/2.5515

[14] Oh, J. Y., Ma, F., Hsieh, S.-Y., and Yang, V., "Interactions Between Shock and Acoustic Waves in a Supersonic Inlet Diffuser," *Journal of Propulsion and Power*, Vol. 21, No. 3, May–June 2005, pp. 486–495. doi:10.2514/1.9671

[15] Greitzer, E. M., "Surge and Rotating Stall in Axial Flow Compressors—Part I: Theoretical Compression System Model," *Journal of Engineering for Power*, Vol. 98, No. 2, April 1976, pp. 190–198.

[16] Mahoney, J. J., *Inlets for Supersonic Missiles*, AIAA Education Series, AIAA, Washington, D. C., 1991.

[17] O'Brian, T. F., Starkey, R. P., and Lewis, M. J., "Quasi-One-Dimensional High-Speed Engine Model with Finite-Rate Chemistry," *Journal of Propulsion and Power*, Vol. 17, No. 6, Nov.–Dec. 2001, pp. 1366–1374. doi:10.2514/2.5889

[18] Farokhi, S., Aircraft Propulsion, Wiley, New York, 2009, pp. 692–702.

[19] Fleifil, M., Annaswamy, A. M., Hathout, J. P., and Ghoniem, A. F., "Reduced-Order Dynamic Models for Control of Reactive Fluid-Flows," *Proceedings of the 38th Conference on Decision and Control*, IEEE Publications, Piscataway, NJ, 1999, pp. 2857–2862.

[20] Ljung, L., "System Identification Toolbox 7 for Use with MATLAB: Reference," MathWorks, Natick, MA, 1995.

[21] Overschee, P. V., and Moor, B. D., "N4SID: Subspace Algorithms for the Identification of Combined Deterministic-Stochastic Systems," *Automatica*, Vol. 30, No. 1, 1994, pp. 75–93. doi:10.1016/0005-1098(94)90230-5

[22] Wang, Q. G., Lee, T. H., Fung, H. W., Bi, Q., and Zhang, Y., "PID Tuning for Improved Performance," *IEEE Transactions on Control Systems Technology*, Vol. 7, No. 4, July 1999, pp. 457–465. doi:10.1109/87.772161

[23] Rivera, D. E., Morari, M., and Skogestad, S., "Internal Model Control. 4. PID Controller Design," *Industrial and Engineering Chemistry Process Design and Development*, Vol. 25, No. 1, 1986, pp. 252–265.

[24] Hoagg, J. B., and Bernstein, D. S., "Nonminimum Phase Zeros: Much to do About Nothing," *IEEE Control Systems Magazine*, Vol. 27, No. 3, June 2007, pp. 45–57. doi:10.1109/MCS.2007.365003

[25] Loove, G., "Rapid Prototyping Using Inversion-Based Control and Object-Oriented Modeling," *Nonlinear Analysis and Synthesis Techniques for Aircraft Control*, edited by D. Bates, Vol. 365, Lecture Notes in Control and Information Sciences, Springer, New York, 2007, pp. 147–173.

[26] Enns, D., Bugajski, D., Hendrick, R., and Stein, G., "Dynamic Inversion: An Evolving Methodology for Flight Control Design," *International Journal of Control*, Vol. 59, No. 1, 1994, pp. 71–91. doi:10.1080/00207179408923070

[27] Raghavendra, P. K., Sahai, T., Kumar, P. A., Chauhan, M., and Ananthkrishnan, N., "Aircraft Spin Recovery, With and Without Thrust Vectoring, Using Nonlinear Dynamic Inversion," *Journal of Aircraft*, Vol. 42, No. 6, 2005, pp. 1492–1503. doi:10.2514/1.12252

[28] Ahsun, U., Merchant, A., Paduano, J. D., and Drela, M., "Design of Near-Isentropic Supersonic Inlet using Active Control," *Journal of Propulsion and Power*, Vol. 21, No. 2, 2005, pp. 292–299. doi:10.2514/1.7709

[29] Moorhouse, D., and Woodcock, R., "Background Information and User Guide for MIL-F-8785C, Military Specification-Flying Qualities of Piloted Airplanes," Flight Dynamic Laboratory ADA119421, July 1982.

[30] Ghosh, K., and Ananthkrishnan, N., "High-Alpha Trim and Stability Analysis of Aircraft Closed-Loop Dynamics with Control Saturation," *International Conference on Nonlinear Problems in Aeronautics and Aviation*, Cambridge Scientific Publications, Cambridge, England, June 2006.

C. Tan
Associate Editor